JOURNAL OF GEOPHYSICAL RESEARCH, VOL. 106, NO. E9, PAGES 20,603–20,620, SEPTEMBER 25, 2001

Tectonics of mascon loading: Resolution of the strike-slip faulting paradox

Andrew M. Freed

Department of Terrestrial Magnetism, Carnegie Institution of Washington, Washington, D. C.

H. Jay Melosh

Lunar and Planetary Laboratory, University of Arizona, Tucson

Sean C. Solomon

Department of Terrestrial Magnetism, Carnegie Institution of Washington, Washington, D. C.

Abstract. Subsidence of lunar mascon maria, impact basins partly filled with mare basalt and sites of prominent positive gravity anomalies, typically led to the formation of concentric graben (arcuate rilles) around the flanks of the basin, while compressive features (mare ridges) formed in interior regions. Although previous numerical models of the response of the lunar lithosphere to mascon loading predict that an annulus of strike-slip faulting should also have formed around mascon maria, no such faults have been observed. This "strike-slip faulting paradox," however, arises from an oversimplification of the earlier models. Viscoelastic finite element models of lunar mascon basins that include the effects of lunar curvature, heterogeneous crustal strength, initial stress conditions, and multistage load histories show that the width of a predicted annulus of strike-slip faulting may be small. The use of Anderson's criterion for predicting fault styles may also overpredict the width of strike-slip faulting. A faulting-style criterion that takes into account transitional faulting, in which both strike-slip and dip-slip components are present, predicts zones of pure strike-slip faulting that are about half of the width predicted by the Anderson criterion. Furthermore, strike-slip faulting should be observed only in regions in which flexural stresses are sufficient to induce rock failure. However, since stress patterns consistent with strike-slip faulting around mascon loads represent a transition between compressional and extensional provinces, differential stresses tend to be low in these regions and for at least part of this region are not sufficient to induce rock failure. A mix of concentric and radial thrust faulting is observed in some mascon maria, at odds with previous models that predict only radial orientations away from the basin center. This apparent discrepancy may be partly explained by the multistage emplacement of mare basalt units, a scenario that leads to a stress pattern where concentric and radial orientations of thrust faults are equally preferred. Detailed models of the Serenitatis basin indicate a 25-km-thick lunar lithosphere at the time of rille formation and a 75-km-thick lithosphere at the time of late-stage mare ridge formation. The extent of observed mare ridges and the inferred cessation of rille formation around Serenitatis prior to the time of emplacement of the youngest mare basalt units is consistent with the superposition of a global horizontal compressive stress field generated by the cooling and contraction of the lunar interior with the local stresses associated with lithospheric loading.

1. Introduction

The response of a planetary lithosphere to a surface load yields insight into the properties of the lithosphere and its state of stress. These insights are often gained by comparing observed surface faulting styles with predictions of numerical models. For example, models have been combined with photogeological observations of faulting to estimate the thickness of the lithosphere beneath lunar mascon loads [*Melosh*, 1978; *Solomon and Head*, 1979, 1980; *Comer et al.*, 1979], Martian volcanoes [*Comer et al.*, 1985; *McGovern and Solomon*, 1993; *Turtle and Melosh*, 1997], and Venusian volcanoes [*McGovern and Solomon*, 1998]. Clearly, our ability to infer lithospheric properties from observed faulting requires that we understand the relationship between faulting style and the state of stress. There are, nonetheless, fundamental deficiencies in our understanding of this relationship. In particular, the response of an elastic plate to

Copyright 2001 by the American Geophysical Union.

Paper number 2000JE001347.
0148-0227/01/2000JE001347$09.00

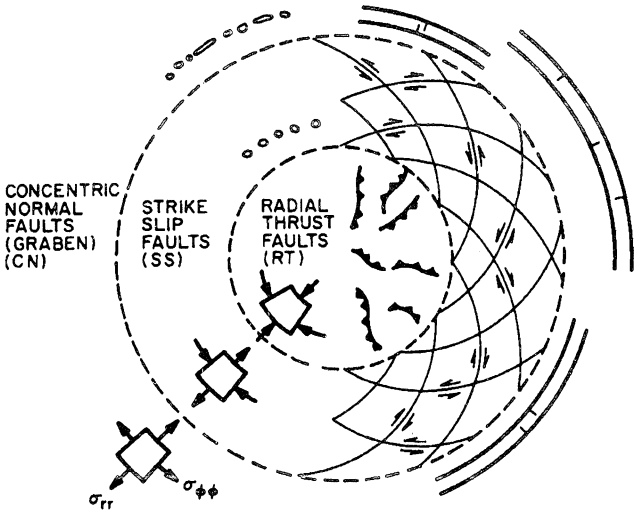

Figure 1. Schematic map view of the surface tectonic style induced by mascon loading [*Melosh*, 1978]. Thrust faults are predicted to occur in the central region, striking approximately radially to the load's center. This region is surrounded by an annulus of strike-slip faults, which is in turn surrounded by concentric normal faults.

an axisymmetric load leads to surface stresses consistent with an inner zone of radial thrust faults, immediately surrounded by an annulus of strike-slip faults, and an outer annulus of concentric normal faults (Figure 1) [*Melosh*, 1978; *Pullan and Lambeck*, 1981; *Willemann and Turcotte*, 1982; *Comer et al.*, 1985; *Janes and Melosh*, 1990; *McGovern and Solomon*, 1993]. The first and third class of features are generally seen, in agreement with simple elastic models. The predicted zone of strike-slip faulting, in contrast, is often not observed. The absence of such predicted features despite the success of loading models to account for other observations has become known as the "strike-slip faulting paradox."

No strike-slip faults, for instance, have been identified on the Moon in association with the subsidence of the mascon mare basins. Within these basins, there are typically wrinkle ridges in the central mare basalt deposits interpreted as the surface expression of thrust or reverse faults [*Howard et al.*, 1973; *Howard and Muehlberger*, 1973; *Muehlberger*, 1974; *Head*, 1974a; *Maxwell et al.*, 1975; *Lucchitta*, 1977]. While some mare ridges have the predicted radial orientation, many ridges tend toward concentric orientations. Normal faulting around mare basins is commonly expressed in the form of linear or arcuate rilles or graben.

The predicted annulus of strike-slip faulting in response to an axisymmetric surface load is a consequence of *Anderson*'s [1951] theory of faulting. In settings in which the vertical stress switches from the minimum to the maximum compressive stress, there should be an intervening region in which the vertical stress is the intermediate compressive stress. Anderson's criterion predicts that strike-slip faulting should develop in such regions, provided that differential stresses are of sufficient magnitude to produce failure. For axisymmetric loads, strike-slip faulting is predicted to occur as sets of conjugate shear fractures trending along Archimedean spirals (Figure 1). This type of fracture pattern would probably involve at most modest displacements, in contrast with large-offset transcurrent or transform faults on Earth.

Several theories for the paucity of observed strike-slip faults in response to surface loads on planetary surfaces have been suggested. *Schultz and Zuber* [1994] suggested that despite the vertical stress being the intermediate principal stress, tension cracks form near the surface and develop into normal faults such that strike-slip faults never form. *Golombek* [1985] suggested that the weak elastic properties of the lunar regolith, in conjunction with an initially nonhydrostatic state of stress, should induce normal faulting at depth that propagates upward to the surface despite a surface stress state conducive to strike-slip faulting. *McGovern and Solomon* [1993] proposed that regions of predicted strike-slip faulting around large volcanoes on Mars failed earlier in normal faulting when the volcanoes were smaller. These normal faults then remain easier to reactivate despite the eventual change in the stress field to one conducive to strike-slip faulting.

In the present study we use a finite element model to explore factors such as planetary curvature, heterogeneous crustal strength, multistage emplacement of mare basalt units, and viscoelastic relaxation processes on the predicted styles of faulting around mascon mare basins. In addition, we consider an alternative criterion for predicting faulting styles. We seek to determine if the failure of previous elastic and analytical models to predict the paucity of observed strike-slip features, as well as the presence of circumferential mare ridges, is the result of neglecting these considerations. Below we first describe the finite element models used in calculations, the significant modeling assumptions, and the criteria used to predict faulting styles from the calculated stress state. We then discuss the influence of each of the principal model parameters on the state of stress. As an application of the insight gained, we then determine a model that accounts for the observed faulting around the Serenitatis basin.

2. Modeling Approach

2.1. Finite Element Models

We simulate the time-dependent loading of lunar mascon basins by mare basalt by means of the finite element code TECTON [*Melosh and Raefsky*, 1980] for a spherical viscoelastic body under axial symmetry. We have validated the TECTON spherical axisymmetric code by comparing numerical solutions to analytical solutions such as that for loading of a self-gravitating uniform sphere. The finite element code can also reproduce the flexural solutions of *Brotchie* [1971] used to model mascon loading by *Solomon and Head* [1979, 1980]. (Note that there is a sign error in the formulations used by *Solomon and Head* [1979, 1980]; the membrane stress N_ϕ/T in their equation A13 and N_θ/T their equation A14 should be negative instead of positive. Our finite element results match the corrected analytical solutions.)

About 18,000 elements are sufficient to model the smooth topographic profiles assumed in constructing the finite element models of mascon basins such as Serenitatis (Figure 2). The axis of symmetry (radial horizontal distance $r = 0$ km) and the outer boundary ($r = 2000$ km) are constrained in the

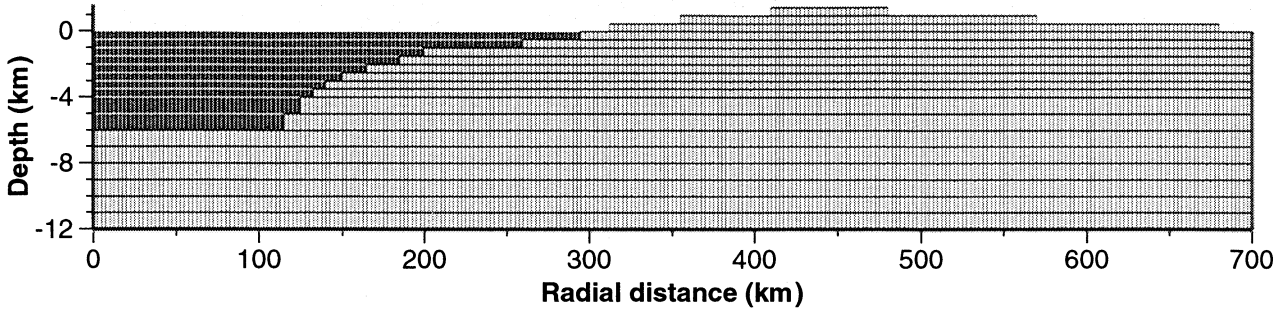

Figure 2. Portion of the axisymmetric finite element model of the lunar mascon basin Serenitatis. The full model extends to 2000 km radial distance and 200 km depth. Nonmare crustal elements are white with black borders; mare basalt elements are black with white borders.

lateral (hoop) direction but are free to move vertically. The bottom boundary is at a depth of 200 km and is fixed. These boundaries are sufficiently distant from the region of deformation in the model that the boundary conditions have no significant influence on model results.

Unless otherwise stated, all models incorporate an elastic lithospheric shell overlying a viscous asthenosphere of viscosity $\eta = 10^{18}$ Pa s. For the purposes of our analysis, the magnitude of the asthenospheric viscosity is not important as long as a steady state solution (i.e., complete relaxation of the asthenosphere) is achieved. Crustal elements, except where noted below, have a modeled density of 2900 kg/m^3. Mantle and mare basalt elements have a modeled density of 3300 kg/m^3. Initially, we consider the elastic strength of the lunar lithosphere to be uniform, with Young's modulus $E = 10^{11}$ Pa and Poisson's ratio $\nu = 0.25$. Later we consider alternative assumptions regarding elastic strength.

Calculations begin with an assumed geometry for an unfilled basin after impact and associated rebound and early relaxation processes [*Melosh*, 1989] are complete but prior to mare basalt fill. We use the Orientale basin as a guide to the characteristics of an unfilled basin [*Solomon and Head*, 1979] by scaling the geometry in proportion to the respective basin ring diameters. Although Orientale has a rather complex geometry, perhaps the result of its location at the boundary between farside highlands and nearside maria [*Williams and Zuber*, 1998], it nevertheless represents a reasonable standard for defining the geometry of an unfilled basin on the basis of is relatively young age and good state of preservation. Figure 2 shows a Serenitatis-sized basin scaled from Orientale topography by inner ring diameter [*Head*, 1979]. The basement geometry of basins partially filled by mare basalt is uncertain, however. Thus we consider several alternative shapes of basin floors, primarily by varying the depth of fill at the basin center. Because basin geometry does vary among models, each parameter study below is accompanied by a figure that shows the modeled basin and load geometry for that study. The effect on the flexural stresses of uncertainties in the magnitudes of mare loads as well as in basin and load geometry is discussed below.

We initially consider the premare stress state beneath and around a mascon basin to be hydrostatic; i.e., all principal stresses are equal to the overburden. Later we consider alternative initial stress states. It is worth noting, however, that most arcuate rilles and all mare ridges occur within mare basalt units, which would not have been influenced by premare stress state, such as that imparted by either partial compensation or overcompensation of basin topography by elevation of the crust-mantle boundary [*Neumann et al.*, 1996]. Even where circumferential rilles cut nonmare units, they are often continuations of faults on mare units [*Solomon and Head*, 1979, 1980], implying that they formed in response to mare loading.

To begin the calculation in a state of hydrostatic stress, surface topography must be supported by either Airy (e.g., Moho topography) or Pratt (laterally varying density structure) isostasy. However, isostatic compensation induces pressure gradients that lead to the viscous removal of any lateral gradients in density at depths greater than that of the brittle/ductile transition or the mechanical lithosphere/asthenosphere boundary. To calculate flexural stresses associated with, for example, a 25-km-thick lithosphere, the depth of compensation in the model cannot exceed 25 km. Such a model could not, for example, incorporate Airy support at a lunar Moho at an average depth of 55 km [*Nakamura et al.*, 1979; *Goins et al.*, 1981]. We instead accomplish this calculation by means of Pratt compensation within the mechanical lithosphere. Though this assumption is not likely to be correct, our results suggest that the form and depth (as opposed to the degree) of premare compensation does not significantly influence the postmare flexural state of stress.

Though finite elements that represent mare basalt are always present in the model, any portion of the mare fill can be effectively removed from the simulation by removing the mass and stiffness of the appropriate elements. We simulate the emplacement of a mare basalt unit by increasing the mass and stiffness of mare basalt elements from zero to their full values in a short time compared with the relaxation time of the underlying asthenosphere. In models that simulate multiple volcanic units within a single basin, we allow flexure due to an early mare unit to achieve steady state (i.e., full relaxation of the asthenosphere) prior to introducing the mass and stiffness of the younger unit.

2.2. Criteria for Predicting Fault Styles

In general, we use *Anderson*'s [1951] criterion to predict faulting styles from the relative order of the magnitude of the three stress components (Figure 3). Anderson's criterion

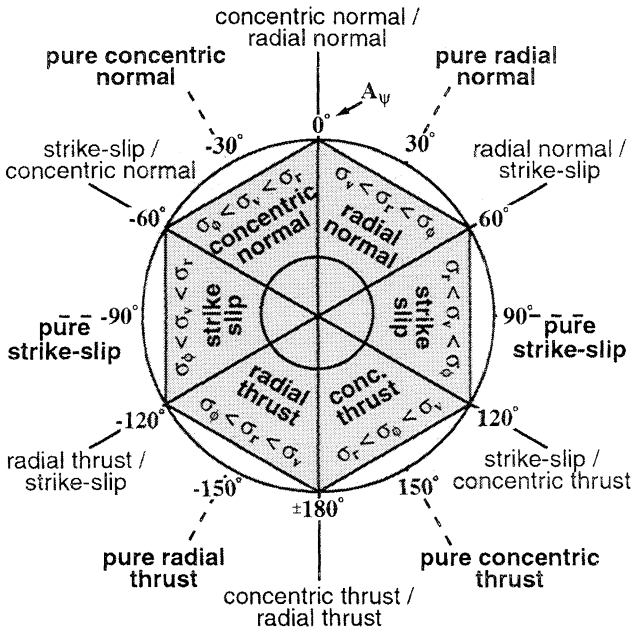

Figure 3. Comparison of predicted faulting-style categories made with the *Anderson* [1951] criterion and with the shape parameter A_ψ (see text). *Anderson*'s [1951] criterion, represented by the gray hexagon, divides predicted faulting styles into six categories on the basis of whether the vertical stress σ_v is the most compressive, least compressive, or intermediate principal stress, as well as the relative magnitude of the radial (σ_r) and circumferential (σ_ϕ) horizontal stresses. The *Anderson* [1951] criterion does not incorporate regions of transitional faulting where slip may have both dip-slip and strike-slip components. The shape-parameter criterion, represented by the circle, also based on the relative magnitude of the principal stresses, considers a continuous spectrum of faulting styles that range from pure strike-slip to pure dip-slip as well as transitional regions that would be expected to occur between such states.

predicts faulting style on the basis of whether the vertical stress σ_v is the most compressive, least compressive, or intermediate principal stress. An example of the correspondence between a calculated stress state and the predicted style of faulting is shown in Figure 4, which shows a typical calculated stress state at the surface ($\sigma_v = 0$) within and near a mare basin in response to a mare basalt load.

Anderson's criterion has shown great utility for understanding and characterizing tectonic regimes and has been applied extensively by geologists because of its ease of use. However, the criterion is an over-simplification in that it ignores transitional or mixed-mode styles in which fault slip contains both strike-slip and dip-slip components. Transitional faulting will occur when two components of the stress tensor are of nearly equal magnitude. For example, in Figure 4 at r = 307 km the hoop and vertical stresses are both zero. In this region we would expect to find normal faults with a significant strike-slip component. For axisymmetric surface loads, transitional faulting also occurs where faults change orientation from radial to concentric, such as at r = 180 km in Figure 4. Here we would expect to find nearly pure thrust faulting, though we might observe a mixture of radial and concentric orientations.

The concept of mixed-mode faulting is of particular importance to a determination of the locus of conjugate shear fractures (strike-slip faulting) around axisymmetric loads. It is unlikely that surface or near-surface faulting with a significant dip-slip component would be recognized photogeologically as conjugate shear fractures. Rather, conjugate shear fractures are more likely to be discerned in regions governed by pure or nearly pure strike-slip faulting, i.e., a region in which the vertical component of stress is the intermediate principal stress by a substantial margin. Thus a criterion for determining where we would expect to observe conjugate shear fractures not only needs to consider locations where the vertical stress is the intermediate principal stress, but also must be able to distinguish transitional faulting from purely strike-slip faulting.

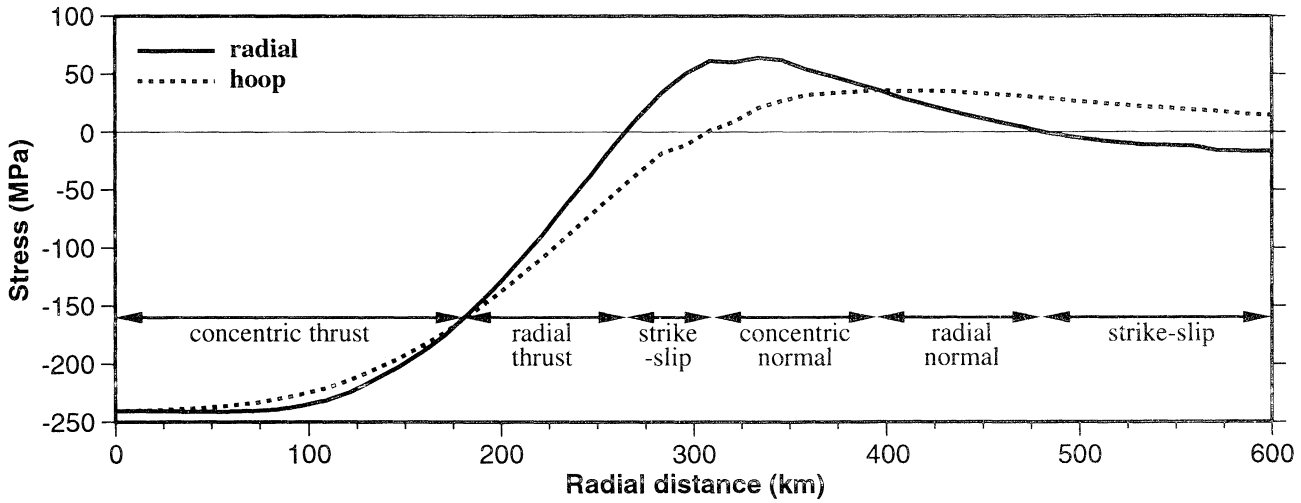

Figure 4. A typical calculated stress state at the surface of a mascon mare basin (basin and load geometry shown in Figure 2). The center of the basin is located at radial distance r = 0. Compressive stresses are negative. The predicted styles of faulting, in accordance with *Anderson*'s [1951] criterion, are determined by whether the vertical stress σ_v is the most compressive, least compressive, or intermediate principal stress. The orientation (concentric or radial) of thrust or normal faults depends on the relative magnitude of the radial and hoop stresses (see Figure 3).

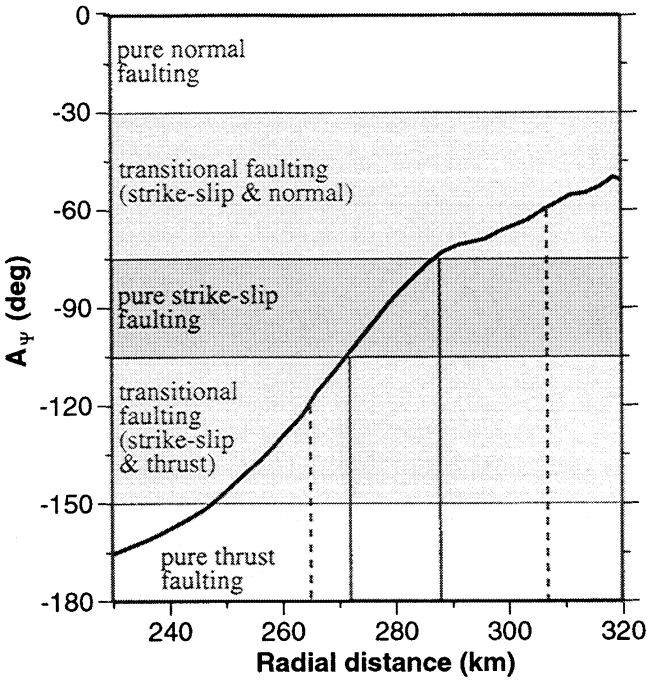

Figure 5. Regions of pure and transitional faulting as determined by the shape parameter, A_ψ [*Simpson*, 1997], defined on the basis of ratios of the principal stresses for the stress state of Figure 4. The vertical solid lines delimit the region in which conjugate shear fractures would be expected to form. Vertical dashed lines define the region of strike-slip faulting predicted by Anderson's criterion.

In recognition of the existence of transitional styles of faulting, Anderson's fault types have been extended and quantified by a number of researchers [e.g., *Philip*, 1987; *Guiraud et al.*, 1989; *Celerier*, 1995]. *Simpson* [1997] used a geometric approach to quantification of fault type based on a shape parameter, A_ψ (degrees). For an axisymmetric surface load the shape parameter is given by

$$A_\psi = \tan^{-1}[(\sigma_{1rv} - \sigma_\phi)/\sqrt{3}(\sigma_{2rv} - P)], \quad (1)$$

where σ_{1rv} and σ_{2rv} are the greatest and least compressive principal stresses on the axisymmetric radial/vertical plane, σ_ϕ is the circumferential principal stress, P is pressure $[(\sigma_{1rv} + \sigma_{2rv} + \sigma_\phi) / 3]$, and compressive stress components are negative. The purpose of the shape parameter is to convey, in a single quantity, information regarding the relative magnitudes of the three components of the stress tensor. Figure 3 shows the correspondence between the shape parameter and the predicted styles of faulting and compares this continuous system to the compartmentalized criterion of *Anderson* [1951].

The calculated shape parameter for the sample surface stress state of Figure 4 is shown in Figure 5 for the radial range $230 < r < 320$ km. The negative A_ψ values indicate that in this region, thrust faults are radial and normal faults are concentric (Figure 3). Pure strike-slip faulting (conjugate shear fractures) is predicted to be observed in the range $272 < r < 288$ km (solid vertical lines). In contrast, Anderson's criterion would predict strike-slip faulting over the wider annulus $264 < r < 307$ km (dashed vertical lines). The range over which one would expect to observe strike-slip faulting thus depends on the criterion used. While the shape parameter helps to differentiate between pure and mixed-mode faulting, the simplicity of Anderson's criterion is often advantageous for illustrating certain points. We therefore utilize both criteria below.

3. Parameter Studies

3.1. Surface Curvature (Planet Radius)

Curvature increases the effective stiffness of a planetary lithosphere. To understand how this increase influences the stress components associated with flexure in response to a mare load, we compare a model that considers lunar curvature to one in which the lithosphere is a flat plate. Both models are for a basin with a radius of 450 km, a mare basalt load that extends to $r = 300$ km and is 4 km thick at the basin center, and a 50-km-thick lithosphere. Flexural stress differences between these models indicate that curvature causes radial stresses near the surface to be more compressive, while hoop stresses become more compressive within and more extensional outside the basin (Figures 6a and 6b).

A curved lunar lithosphere results in a smaller region on the flank of the basin in which the vertical stress is the intermediate stress and thus a smaller predicted region of strike-slip faulting. (Compare Figures 6c and 6d, but note that the lunar curvature is not shown in Figure 6d and subsequent figures for ease of comparing results.) The model that includes lunar curvature predicts a region of strike-slip faulting only 90 km wide (Anderson's criterion) compared with a 220-km-wide region for the flat model. For comparison, the shape-parameter criterion predicts a region of conjugate shear fractures only 45 km wide for the curved model. Thus, for this example, we have reduced the 220-km-width of the predicted annulus of strike-slip faulting from a flat model incorporating Anderson's criterion by a factor of ~5 simply by considering the influence of lunar curvature and the shape-parameter criterion.

Many stress models (including those in Figure 6) show that stress orientations consistent with strike-slip faulting are predicted not only on the flank of the basin, but also well outboard of the flank ($r > 630$ km in Figure 6). However, as discussed below, the magnitude of stress in these outer regions is not sufficient to induce failure. Unless otherwise stated, the term strike-slip region in this study always refers to the region on the basin flank.

We explore further the influence of planetary curvature on the width of the annulus of strike-slip faulting by considering a series of models in which we vary the planet radius. Figure 7 compares the predicted width of the annulus of strike-slip faulting due to loading if the basin shown in Figure 6 were located on any of the inner planets, the Moon, Saturn's moon Iapetus (chosen for its small size), and two fictitious planets (selected for completeness). In each of the models we used the known surface gravitational attraction of the planet. For the fictitious planets we used a gravitational attraction corresponding to an average density equal to that of the Moon. The results demonstrate that decreasing planet radius (increasing surface curvature) leads to a decrease in the width of the region of predicted strike-slip faulting. For the model used in this study, no strike-slip faulting should be

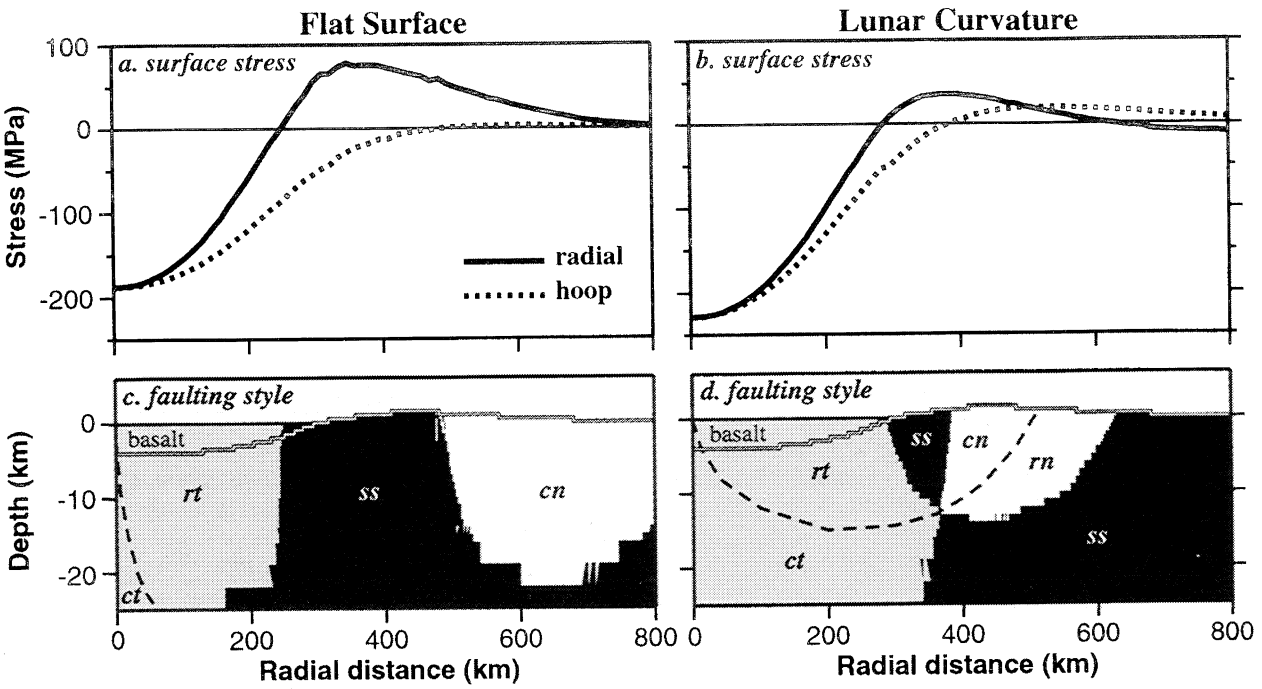

Figure 6. The effect of lunar curvature on stress induced by loading of a mare basin by basalt fill, for a 50-km-thick elastic lithosphere and a mare load that is 4 km deep in the center and extends to 300-km radial distance. (a,b) Calculated surface stress and (c,d) styles of faulting in the upper lithosphere in accordance with Anderson's criterion are shown for a model with a (left) flat surface and for one that includes (right) lunar curvature. Compressive stresses are negative. Regions of predicted strike-slip faulting (ss) are shown in black. Regions of predicted radial thrust (rt) and concentric thrust (ct) faulting are shown in gray. Regions of concentric normal (cn) and radial normal (rn) faulting are shown in white.

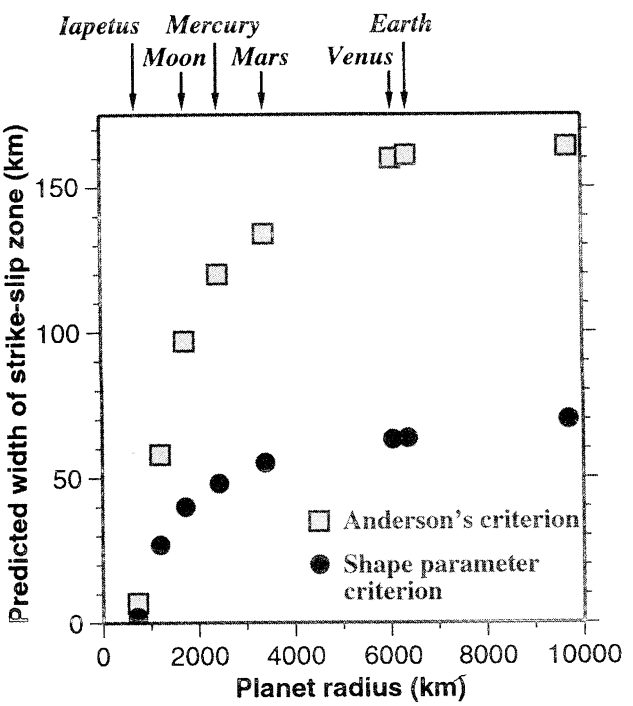

Figure 7. Predicted width of the annulus of strike-slip faulting in response to loading of the basin shown in Figure 6 as a function of planet radius, for both Anderson's criterion and the shape-parameter criterion. Regardless of the criterion used, the predicted width of the annulus of strike-slip faulting decreases with decreasing planet radius (increasing surface curvature).

induced if the planet radius is less than about 750 km. Varying the gravitational attraction, for a fixed curvature, modifies the stress magnitudes resulting from loading but does not influence the wavelength of deformation or the predicted styles of faulting.

3.2. Lithosphere Thickness

The thickness of the elastic lithosphere significantly influences the magnitude and wavelength of surface deformation in response to a mare load, because the flexural rigidity of the lithosphere, a measure of the lithospheric stiffness, is proportional to the cube of the lithosphere thickness [*Turcotte and Schubert*, 1982]. For the mare basin model of Figure 6d we compared flexural stresses for a 100-km-thick lithosphere to those for a 25-km-thick lithosphere. As shown in Figures 8a and 8b, a thinner lithosphere leads to an increase in the magnitude of stresses.

From the standpoint of predicting faulting styles, a thinner lithosphere leads to a decrease in the wavelength of deformation and a much smaller region in which the vertical stress is the intermediate surface stress on the flank of the basin. Thus the radial extent of predicted strike-slip faulting at the flank of the basin is reduced in the model with a thinner lithosphere. Compare the difference in predicted styles of faulting between the two models shown in Figures 8c and 8d. For the 25-km-thick lithosphere the predicted annulus of strike-slip faulting is only 45 km wide. The relationship between the width of the strike-slip zone and lithosphere thickness is further clarified by considering a range of models in which the lithosphere thickness varies from 25 to 150 km. As shown in Figure 9, the dependence of the width of the

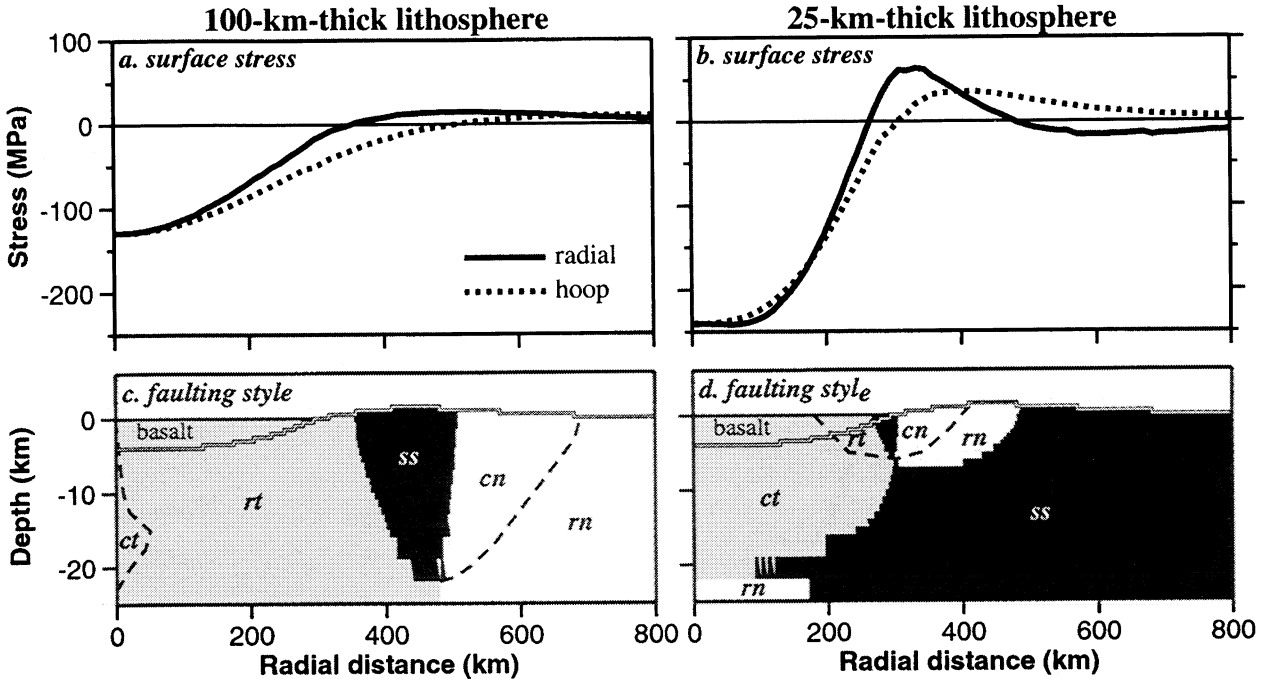

Figure 8. The effect of lithosphere thickness on stress induced by loading of a mare load that is 4 km deep in the basin center and extends to 300 km radial distance. (a,b) Calculated surface stress and (c,d) styles of faulting in the upper lithosphere in accordance with Anderson's criterion are shown for a (left) 100-km-thick lithosphere and a (right) 25-km-thick lithosphere. Lunar curvature is included. Other conventions follow Figure 6.

strike-slip zone to lithospheric thickness is similar to that of planetary curvature (Figure 7).

With the shape-parameter criterion the region within which we would expect to observe conjugate shear fractures associated with flexure of a 25-km-thick lithosphere is an annulus only 15 km wide. Thus, by including surface curvature, a potentially thin lithosphere at the time of basin loading, and the shape-parameter criterion, we have reduced the region of strike-slip faulting in Figure 6c by a factor of 15.

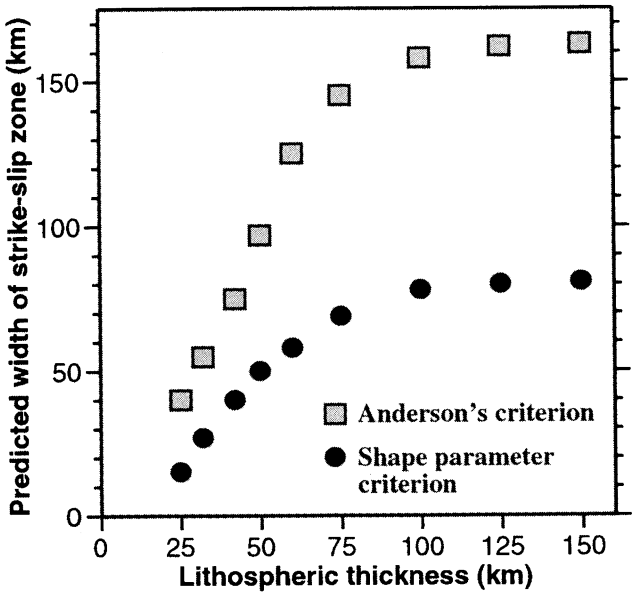

Figure 9. Predicted width of the annulus of strike-slip faulting in response to loading of a mare basin by mare basalt fill as a function of lithospheric thickness. All models incorporate a 450-km-wide basin, a mare load that is 4 km deep at the center and extends to 300-km radial distance, and lunar curvature.

In addition to influencing the width of the strike-slip zone, lithosphere thickness also influences the location of normal faulting. For the 100-km-thick lithosphere, normal faulting is predicted to occur only outward of 500 km from the basin center (Figure 8c). In contrast, normal faulting is predicted to occur inward to 300 km radius for a 25-km-thick lithosphere (Figure 8d). Thus the observed location of concentric rilles around mare basins can be used as an indicator of the thickness of the lithosphere at the time of rille formation [*Solomon and Head*, 1979, 1980; *Comer et al.*, 1979].

It is probable that the flexural rigidity of the lunar lithosphere was laterally heterogeneous beneath a lunar basin immediately following basin formation, the result of localization of subsurface heating by the impact. Lateral variations in subsurface temperature generally lessened with time by the conductive loss of impact-generated heating [e.g., *Bratt et al.*, 1985b]. To understand the influence of lateral heterogeneity of lithospheric thickness we considered models in which lithospheric thickness increased from 25 km at the basin center to 50 km at large radial distances; both the location and width of the transition zone were varied. Our results agreed with the analytical solutions of *Pullan and Lambeck* [1981], who found that if the thin portion of the lithosphere is confined to a radius much smaller than the load radius, its presence is not significant. If the thinner portion of the lithosphere is comparable in radial extent to the load, then the resulting stress field looks similar to the results from a lithosphere with a uniform, intermediate thickness. For

example, in the case of a 300-km-wide, mare-filled basin with a lithospheric thickness that varies from 25 km at 200 km form the basin center to 50 km at 300 km from the basin center, the overall stress pattern looks similar to that of a model with a uniform 40-km-thick lithosphere. The width of the strike-slip zone, however, extends farther inward in the heterogeneous model than in a uniform-lithosphere model. This effect reflects differences in the stress field within in the transition region. The overall similarity of results for uniform- and heterogeneous-lithosphere models makes it unlikely that observed faulting styles at mascon basins can discriminate between model types.

3.3. Basin and Mare-Fill Geometry

Mascon mare basins range in diameter from 430 km (Grimaldi) to 1500 km (Imbrium), and the fraction of the basin diameter covered by mare basalt varies between 20 (Humboldtianum) and 87 (Fecunditatis) percent [*Wilhelms*, 1987]. While basin diameter and radial extent of mare fill are readily observed, the thickness of mare basalt must be inferred from other data sources, may include intrusions as well as surface flows, and is therefore not known. For example, *Solomon and Head* [1979] assumed that the topography of the nearly unfilled Orientale basin is proportionally representative of the basement geometry of Serenitatis and calculated a mare thickness at the center of Serenitatis of 8.5 km. In contrast, on the basis of a statistical analysis of the depth/diameter ratio for 29 large lunar craters and basins, *Williams and Zuber* [1998] estimated the thickness of mare basalt at the center of Serenitatis to be 4.3 km. *Budney and Lucey* [1998] used observations of nonmare material excavated by mare craters to estimate mare thickness in Mare Humorum; thickness values were less than those adopted by *Solomon and Head* [1980] for Humorum on the basis of scaling from Orientale. Here we seek to determine the influence of mare load magnitude and other geometric characteristics of basin and mare geometry on styles of faulting induced by flexure.

We consider several models of mascon mare basins that vary in basin and mare basalt geometry. The first model (Figure 10a) is for a relatively small basin 225 km in radius with a mare load 150 km in radius and 4 km in central thickness. The second model (Figure 10b) has mare fill to a radius similar to the first model, but half the mare load, within a relatively large basin of 600 km radius. The third model (Figure 10c) includes the same large basin as the second but is filled by mare basalt nearly to 450 km radius and to a 4-km central thickness. The final model (Figure 10d) incorporates a large basin (600 km radius) filled to a 6-km thickness in the center but only to 0.5 km within the outer region of mare fill (250 km $< r <$ 450 km). The third and fourth models would look identical in map view.

A comparison between Figures 10a and 10b shows that increasing the radius of the basin but not the radius of the mare load leads to relatively similar predicted styles of faulting, even if the thickness of the mare loads are not of similar magnitude. However, a comparison between Figures 10b and 10c shows that increasing the radius of the mare load but not the radius of the basin leads to a significant difference in predicted faulting styles. The radius of the load thus has an important influence on the faulting style, while the radius and shape of the basin and the thickness of the load are secondary factors.

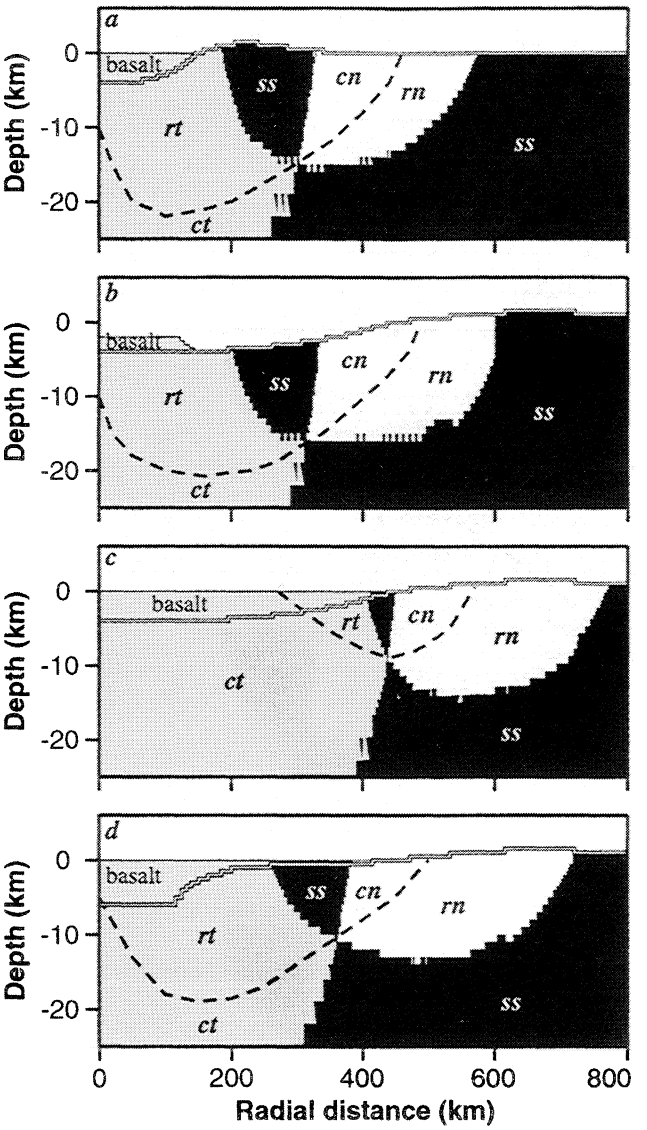

Figure 10. Styles of faulting predicted by Anderson's criterion for four basin configurations: (a) a basin 225 km in radius with a 150-km-radius mare load having a 4-km central depth; (b) a 600-km-radius basin with a 150-km-radius mare load having a 2-km central depth; (c) a 600-km-radius basin with a 450-km-radius mare load having a 4-km central depth; and (d) a 600-km-radius basin with a 450-km-radius mare load having a 6-km central depth with the majority of the load concentrated within 150 km of the basin center. All models include lunar curvature and a 50-km-thick lithosphere. Other conventions follow Figure 6.

The distribution of mare fill also has an important influence on faulting styles. The model with thin fill in the outer mare (Figure 10d) behaves similar to the models with smaller fill radii (Figures 10a and 10b). This result is important to recognize, because many of the basins are likely to have relatively shallow mare fill in their outer regions [*Solomon and Head*, 1980]. In addition, this comparison suggests that if large and dense basaltic intrusions lie beneath the basin floor and have a distribution significantly different from the surface fill (e.g., concentrated as a central plug), the styles of faulting resulting from flexure could be

significantly altered from the case where the load distribution is fully determined by mare fill geometry.

As shown by the comparison between Figures 10a and 10c, the larger the radius of the mare load, the smaller the width of the predicted strike-slip zone (for a comparable ratio of mare fill radius to basin radius). Consideration of a range of models shows that the width of the annulus of strike-slip faulting decreases approximately linearly with increasing load radius. The physical explanation of this result is that a larger load radius samples a larger portion of the lunar circumference and therefore is more greatly influenced by planetary curvature. This conclusion is supported by the observation that increasing the load radius does not significantly influence the predicted width of strike-slip faulting when a flat surface is assumed.

The lack of influence of the radius of the basin itself (independent of mare load) on the faulting pattern results from the fact that the effective stiffness of the lithosphere is not significantly altered by changing the horizontal extent of a depression 4-6 km deep, even if the lithosphere is only 25 km thick. Basin geometry is probably influential only when the lithosphere is relatively thin, perhaps 15 km or less. The insensitivity of the flexural stress field to pre-fill basin geometry permits us to model multiring basins without having to consider details of the basin profile. For example, a Serenitatis basin geometry that includes three positive-relief rings instead of one produced nearly the same flexural stresses and predicted styles of faulting as the model with smoothed topography.

3.4. Generalized Relation for the Predicted Width of an Annulus of Strike-Slip Faulting

Landau and Lifshitz [1970] suggest that a major portion of the elastic energy induced by a point load on a thin-walled sphere is concentrated in a narrow annulus near the edge of the load-induced depression. They refer to this region as the "bending strip" (labeled w_a in the inset of Figure 11), where bending is accompanied by a transition from compressional to extensional horizontal stresses outward from the depression along the outer face of the sphere. Furthermore, they find that the width of the bending strip is proportional to the square root of the radius of the sphere and to the square root of the thickness of the shell. This description is analogous to the predicted width of the annulus of strike-slip faulting near mascon loads. As with the bending strip, the strike-slip zone represents a region of transition from compressional to extensional horizontal stresses, and our models also show an approximate square root relationship between the width of the strike-slip zone and both the planetary radius (Figure 7) and the lithospheric thickness (Figure 9).

This relationship is further explored in Figure 11, in which the width w_a of the strike-slip zone given by *Anderson*'s [1951] criterion is plotted against the square root of the product of planet radius R and the lithospheric thickness T. As shown in Figure 11, the width of the strike-slip zone is also influenced by the load radius r_L. The relationship between the predicted width of the strike-slip zone and all three parameters can be collapsed into a single approximation given by

$$w_a \approx 0.5\,(R\,T)^{1/2} - r_L/3. \qquad (2)$$

This expression provides a good estimate of the width of the strike-slip zone, without the need for a more detailed numerical calculation, for most of the mascon load geometries adopted in this paper. An exception is the mascon load geometry shown in Figure 10d, for which (2) overcorrects for the radial extent of the thin distal portion of the mare fill.

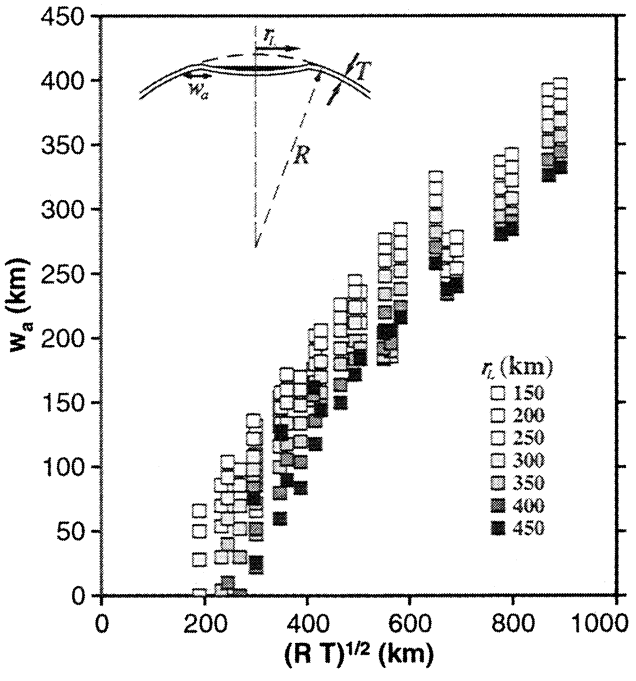

Figure 11. Predicted width of an annulus of strike-slip faulting given by the Anderson faulting criterion (w_a) for a mascon load of radius r_L as a function of planet radius (R) and lithosphere thickness (T). Inset shows a schematic view of basin deformation adapted from *Landau and Lifshitz* [1970], who considered w_a as a "bending strip" that occurs on the edge of the depression induced by a point load on a sphere. In the mascon loading problem the mare basalt fill (black) replaces a point load. This schematic provides a basis for the development of a simple analytical expression (equation (2)) for the predicted width of a strike-slip zone without a need for a detailed numerical calculation (see text).

If we presume that strike-slip faulting (pairs of conjugate shear fractures) will be observable only if the fault slip does not include a significant dip-slip component, then it would be more appropriate to consider the width of pure-strike slip faulting predicted by the shape parameter. This reasoning leads to the alternate relation

$$w_s \approx 0.25\,(R\,T)^{1/2} - r_L/6. \qquad (3)$$

For a mare load 300 km in radial extent (e.g., Serenitatis) on the Moon (R = 1738 km) with a lithospheric thickness of 50 km, for example, (3) predicts a width for the annulus of strike-slip faulting of ~25 km. For a load of the same extent on Venus, in contrast, the width of the predicted zone of strike-slip faulting, for the same lithosphere thickness, is ~90 km. This difference may explain the fact that while strike-slip faulting has not been observed on the Moon, pairs of conjugate shear fractures have been reported around at least one corona on Venus [*Willis and Hansen*, 1996]. It should be noted that the probable internal structure and inferred sequence of deformational episodes at the generally circular

corona structures on Venus differ from those at lunar mascon maria [e.g., *Stofan et al.*, 1992; *Squyres et al.*, 1992, *Janes et al.*, 1992]. Nonetheless, confirmation of strike-slip faulting around coronae on Venus would represent the first such faulting documented for a circular surface feature on a solar system object.

3.5. Premare Compensation Levels

Isostatic equilibrium represents a state in which pressures caused by the weight of overlying rock balance at some depth beneath the surface. This is the state to which planetary topography tends to evolve and is indicated by a free-air gravity anomaly that is poorly correlated with topography, as in the case of the lunar highlands [e.g., *Zuber et al.*, 1994]. In contrast, most nearside mare basins display large positive free-air anomalies indicating large departures from local compensation [*Muller and Sjogren*, 1968]. These mascon anomalies arise in part from the effects of impact processes [e.g., *Wise and Yates*, 1970; *Bowin et al.*, 1975; *Phillips and Dvorak*, 1981] and in part from subsequent volcanic filling by mare basalt that is denser than the surrounding crust [*Conel and Holstrom*, 1968; *Phillips et al.*, 1972; *Bratt et al.*, 1985a]. While both mare fill and an elevated crust-mantle boundary likely contribute to the observed gravity [*Zuber et al.*, 1994, *Neumann et al.*, 1996], the relative importance of each is uncertain because of poor knowledge of density heterogenieties in the crust and, as previously discussed, uncertainties in the thickness of mare basalts that at least partially fill the nearside mascon basins. As a result, there is uncertainty regarding premare isostatic compensation levels and therefore the premare state of stress. The premare stress state, if not hydrostatic, might have an important influence on the final stress state following flexure due to mare loads.

If impact and early relaxation processes led to a density structure that undercompensates basin relief, later uplift of the basin region would have occurred [*Melosh*, 1976]. We simulated this uplift process by postulating a density structure that compensates only 50% of basin relief, then allowing the viscous asthenosphere to relax. The results are not influenced by the type or depth of compensation, only the degree of compensation and the thickness of the elastic lithosphere. Figure 12a shows the styles of faulting predicted by Anderson's criterion after uplift (upward deflection not shown) of an initially 50%-compensated Serenitatis basin for a 25-km-thick lithosphere. Uplift induces flexural stresses in the crust that are opposite in sign to those of subsidence and thus induce faulting in an opposite sense, normal faulting within the basin and thrust faulting on the outer flanks. The superposition of flexural stresses due to uplift and those due to mare loading would tend to cancel, though the wavelengths governing the two processes may differ.

In contrast, impact and early relaxation processes could have led to a density structure that overcompensated basin topography. For example, *Neumann et al.* [1996] interpret gravity anomalies for the Orientale basin as suggesting a very large upward deflection of the crust-mantle boundary leading to overcompensation. This excess load would have caused a subsidence of the lithosphere similar to that due to a mare load. Figure 12b shows the predicted styles of faulting associated with a basin that has been overcompensated by a factor of 1.5. Stresses due to overcompensation would add to those due to a subsequent mare load, inducing higher levels of stress than would be expected from only the mare load.

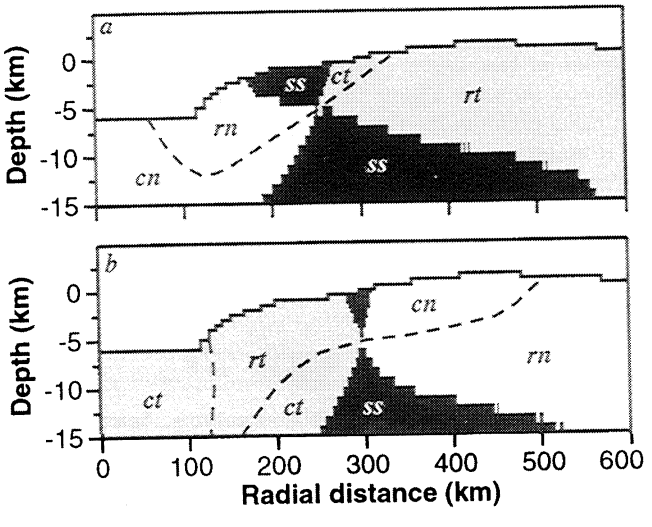

Figure 12. Styles of faulting predicted by Anderson's criterion following (a) uplift of an unfilled impact basin due to undercompensated topography and (b) subsidence of an unfilled impact basin due to overcompensated topography following impact and early relaxation processes. Deflections are not shown. Both models include lunar curvature and a 25-km-thick lithosphere. Other conventions follow Figure 6.

3.6. History of Mare Emplacement

Most mare basins show evidence that filling by volcanism occurred in stages, usually with early basalt units comprising the bulk of the total fill volume [*Pieters et al.*, 1975, 1980; *Head*, 1974b; *Head et al.*, 1978; *Whitford-Stark and Head*, 1980; *Solomon and Head*, 1980; *Wilhelms*, 1987]. Early mare volcanism is inferred to have influenced rille formation prior to ~3.6 b.y. ago [*Lucchitta and Watkins*, 1978], while mare ridge formation continued after volcanism as recent as 3.0 b. y. ago [*Solomon and Head*, 1979, 1980]. If a basalt unit is emplaced after all basin subsidence induced by an older mare load has been completed, the younger unit will not experience the bending stresses associated with this earlier flexure. Thus mare units of distinct ages may manifest different stress states and associated styles of faulting.

To study the significance of volcanic history on flexural stresses we considered two models of mascon loading that differ in the timing of basalt deposits. In the first model we consider a mascon basin in which all of the mare basalt was deposited at the same time, thus causing a single flexural event. In the second model we assume that the top 1 km of mare basalt was emplaced after a larger earlier basalt unit (5 km thick at basin center) had been deposited and the flexural response to this lower unit had already achieved steady state. Thus the second model simulates two distinct flexural events. As shown in Figure 13a, the first model leads to stresses in the upper mare basalt ~7 times larger (at basin center) than those of the second model. The difference in stress magnitudes is due to the insensitivity of the upper mare basalt unit to flexure induced by the lower unit in the second model.

The history of mare volcanism not only influences the magnitude of stresses in the upper mare units, but also

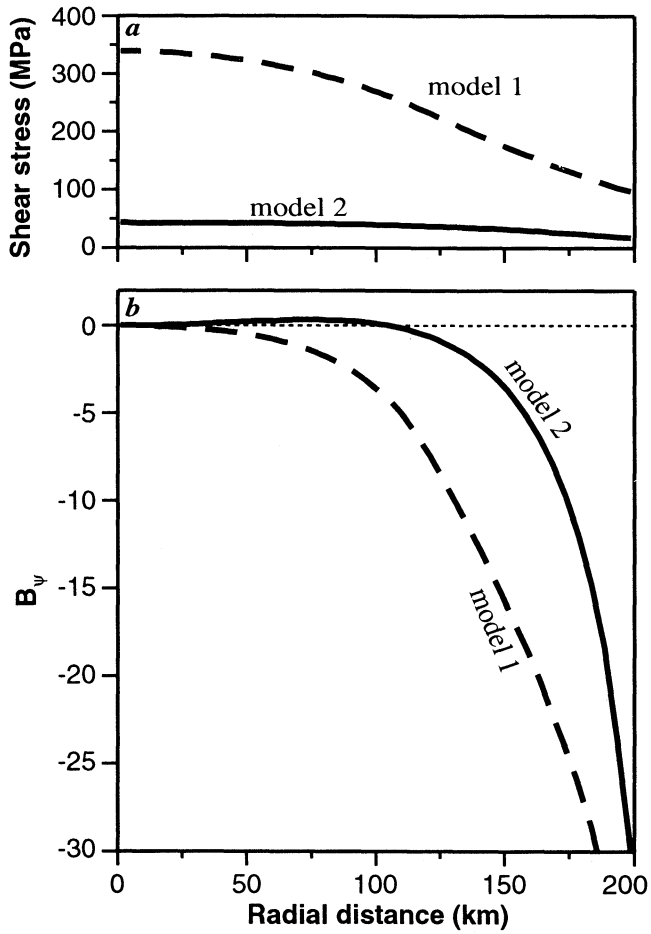

Figure 13. (a) Shear stress in the center of a 1-km-thick top unit of mare basalt induced by the loading of a 450-km-radius mascon basin by a mare load that is 6 km deep in the center and extends to 300 km radial distance. In model 1, all of the mare basalt is deposited as a single unit. In model 2, the 1-km-thick top unit is deposited after flexure due to lower units had already achieved steady state. Both models include a lithospheric thickness of 25 km and lunar curvature. (b) Modified shape-parameter B_ψ (equation (4)) within the top layer of mare basalt for the two models. Radially oriented thrust faulting is predicted to occur at $B_\psi = -30^o$, concentrically oriented thrust faulting occurs at $B_\psi = 30^o$, and the cross-over where neither orientation is preferred occurs at $B_\psi = 0^o$.

whether thrust faulting should be oriented radially or circumferentially. The sensitivity of orientation to load history can be shown by plotting the shape parameter as a function of radial distance from the basin center for the two models. However, since the change from radially oriented thrust faults to circumferentially oriented thrust faults involves a cross-over of A_ψ from 180^o to -180^o (Figure 3), a plot of A_ψ is discontinuous within the thrust faulting regime. Therefore, for graphical purposes we define a new parameter B_ψ

$$\begin{aligned} B_\psi &= 180^o - A_\psi \qquad A_\psi > 0, \\ B_\psi &= -180^o + A_\psi \qquad A_\psi < 0. \end{aligned} \tag{4}$$

With this definition, radially oriented thrust faulting is predicted to occur near $B_\psi = -30^o$, concentrically oriented thrust faulting occurs near $B_\psi = 30^o$, and the cross-over where neither orientation is preferred occurs at $B_\psi = 0^o$.

For the model in which mare basalt was deposited as a single unit (model 1), radially oriented thrust faults become the preferred orientation at radial distances greater than ~100 km from the basin center (Figure 13b). For model 2, in which the upper mare basalt unit was deposited well after the lower unit, the preference for radially oriented thrust faults has moved farther from the basin center, to radial distances greater than 150 km. These results suggest that the observed mixture of radially and circumferentially oriented thrust faults in the mascon maria, as opposed to solely radial thrust faults, may be at least partially the result of the uppermost mare basalt units having been deposited long after flexure induced by the load of the lower units had achieved steady state.

4. Application to Mare Serenitatis

Having gained some general insight into the influence of various parameters on faulting styles around mascon basins, we now seek to develop a specific model for Mare Serenitatis. Our objective is to develop a model from which to infer the effective strength of the lunar lithosphere, including the elastic modulus, brittle strength, and lithospheric thickness at the time of rille and ridge formation. The geometry of the Serenitatis basin, ~440 km in radius [*Head*, 1979], is shown in Plate 1. We model the mare fill geometry after *Solomon and Head* [1979], who suggest a 6-km-thick lower unit at the time of rille formation and a 2-km-thick upper unit at the time of youngest mare ridge formation (Plate 1 only shows the lower mare basalt unit). As discussed previously, overestimation of the thickness of the mare basalt fill will not greatly influence the predicted styles of faulting unless the assumed load distribution has significant error. Concentrically oriented arcuate rilles are observed in the mare and on the flank of Serenitatis at radial distances between 250 and 400 km from the basin center [*Solomon and Head*, 1979]. Rilles may have once extended farther inward, but if so such features would be covered by younger flows. Mare ridges are observed from the basin center to a radius of about 300 km. The most distal 50 km of ridges are superimposed on older rilles. This relationship indicates that times of rille and ridge formation differ and suggests that rille formation had ceased prior to the formation of many ridges. We follow the argument of *Solomon and Head* [1979] that rilles and ridges associated with Serenitatis were principally the result of lithospheric flexure.

4.1. Elastic Modulus

The flexural response of the lithosphere to a surface load is influenced by the lithosphere's flexural rigidity, $D = E T^3 / (12[1-\nu^2])$, where E is Young's (elastic) modulus, T is the lithosphere thickness, and ν is Poisson's ratio [e.g., *Turcotte and Schubert*, 1982]. Because flexural rigidity is most significantly influenced by variations in lithospheric thickness, most previous analyses of mascon loading [e.g., *Melosh*, 1978; *Comer et al.*, 1979; *Solomon and Head*, 1980] involved assuming values for E and ν and then choosing the lithospheric thickness that best explained observed surface faulting. Here we wish to explore the significance of varying the modeled elastic modulus on the predicted of styles of

faulting. Previous analytical solutions were generally restricted to an elastically homogeneous lithosphere, and a relatively large Young's modulus of 10^{11} Pa was typically assumed. However, the outer 20 km of the present lunar crust and mare basalt may have a modulus less than 10^{11} Pa by a factor of up to 5-20, with the regolith (top 1-3 km) having a modulus as low as 5 x 10^9 Pa [*Pritchard and Stevenson*, 2000] (Plate 1b inset).

To explore the potential influence of an elastically weak outer crust, we consider several models of the Serenitatis basin at the time of rille formation, each with a lithospheric thickness of 25 km. In the first model we assume a uniformly strong elastic lithosphere with a Young's modulus of 10^{11} Pa. In a second model we adopt the weaker elastic modulus profile suggested by *Pritchard and Stevenson* [2000] for both the mare basalt and the nonmare lunar crust. Plates 1a and 1b show predicted faulting styles associated with flexure in response to the mare load for these two models (the zones of predicted rock failure shown in these figures are discussed in the next section). Both models do a reasonably good job of predicting the region of observed concentric normal faults, though portions of this region are calculated to be in transition zones between concentric normal and strike-slip faulting or concentric normal and radial normal faulting. The elastically weaker model (Plate 1b) extends the predicted zones of normal and strike-slip faulting inward toward the basin center, because the effective thickness of the lithosphere in this model is reduced. It is difficult to characterize which of these two models is preferable, because any faulting that occurred inboard of ~250 km from the basin center at the time of rille formation has been covered by younger flows (not shown in Plate 1).

The regolith occupying the outermost 1-3 km of lunar crust consists of ejecta and impact gardened material that may have developed with a Poisson state of stress [*Golombek*, 1985] in which lateral stresses equal one third the overburden. We thus consider a Serenitatis model at the time of rille formation in which the outer 3 km of crust had a Poisson state of stress prior to mare fill. Predicted faulting styles for this model, which also incorporates the weaker modulus of *Pritchard and Stevenson* [2000], is shown in Plate 1c. The initial Poisson stress state influences faulting styles in the top 3 km of crust. Most notably, the region of predicted concentric normal faulting is extended inward. The initial Poisson stress model predicts a stress field at the edge of the basin consistent with normal faulting at shallow depths and strike-slip faulting at the surface. *Golombek* [1985] hypothesized that normal faults initiated at depth could propagate to the surface despite the fact that the surface stresses satisfied conditions for strike-slip faulting. This deeper fault-initiation process might significantly reduce the observed extent of strike-slip faulting around mascon basins.

4.2. Brittle Strength

The brittle strength of the lunar crust is not well constrained. This uncertainty is due to difficulty in extrapolating empirical strength envelopes [e.g., *Byerlee*, 1967] to large-scale faulting [*Scholz*, 1990] and to the uncertainty in the magnitude of the stress field. Previous estimates of the cohesive strength of the outer lunar crust have varied from nearly zero [*Golombek and McGill*, 1983] to at least 20 MPa [*Solomon and Head*, 1979]. The difference in these estimates reflects primarily the respective assumptions regarding the elastic modulus of the outer crust, which strongly influence the magnitude of calculated flexural stresses.

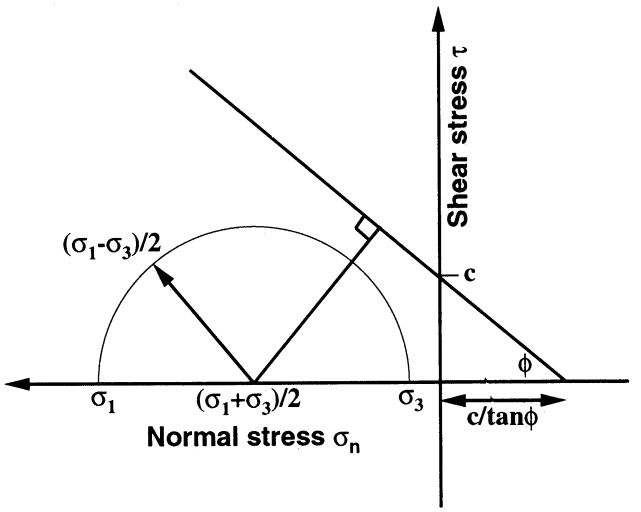

Figure 14. Mohr circle construction demonstrating the concept of proximity to failure.

We relate flexural stresses to rock strength using a Mohr-Coulomb failure envelope (Figure 14). This methodology is predicated on a linear relationship between the shear stress τ and the normal stress σ_n on a fault:

$$\tau_{failure} = c - \sigma_n \tan\phi, \tag{5}$$

where $\tau_{failure}$ is the shear stress on the fault at failure, c is the cohesive strength of the rock, and ϕ is the angle of internal friction. Mohr-Coulomb theory has been used in many previous studies of stresses associated with axisymmetric surface loads [*Melosh*, 1976, 1978; *Hall et al.*, 1986; *McGovern and Solomon*, 1993]. The choice of an alternate failure criterion, such as modified Griffith [e.g., *Secor*, 1965] or Hoek-Brown [*Hoek and Brown*, 1980], would not alter our conclusions, as strength parameters for each of these criteria can be found that yield similar results. By the Mohr-Coulomb criterion, failure occurs when the radius of the Mohr circle $(\sigma_1-\sigma_3)/2$ is equal to the perpendicular distance from the center of the circle at $(\sigma_1+\sigma_3)/2$ to the failure envelope:

$$\left(\frac{\sigma_1-\sigma_3}{2}\right)_{failure} = c\cos\phi - \left(\frac{\sigma_1+\sigma_3}{2}\right)\sin\phi, \tag{6}$$

where σ_1 and σ_3 are the greatest and least compressive principal stresses, respectively. Comparison of stress state and rock strength is facilitated by the concept of proximity to failure P_f, defined as the ratio between the actual radius of the Mohr circle, $(\sigma_1-\sigma_3)/2$, and the radius at failure [*Melosh and Williams*, 1989]:

$$P_f = \left(\frac{\sigma_1-\sigma_3}{2}\right) \Big/ \left(\frac{\sigma_1-\sigma_3}{2}\right)_{failure}. \tag{7}$$

Failure occurs when $P_f \geq 1$.

For each of the models shown in Plate 1, we determined a brittle strength envelope that leads to the prediction that

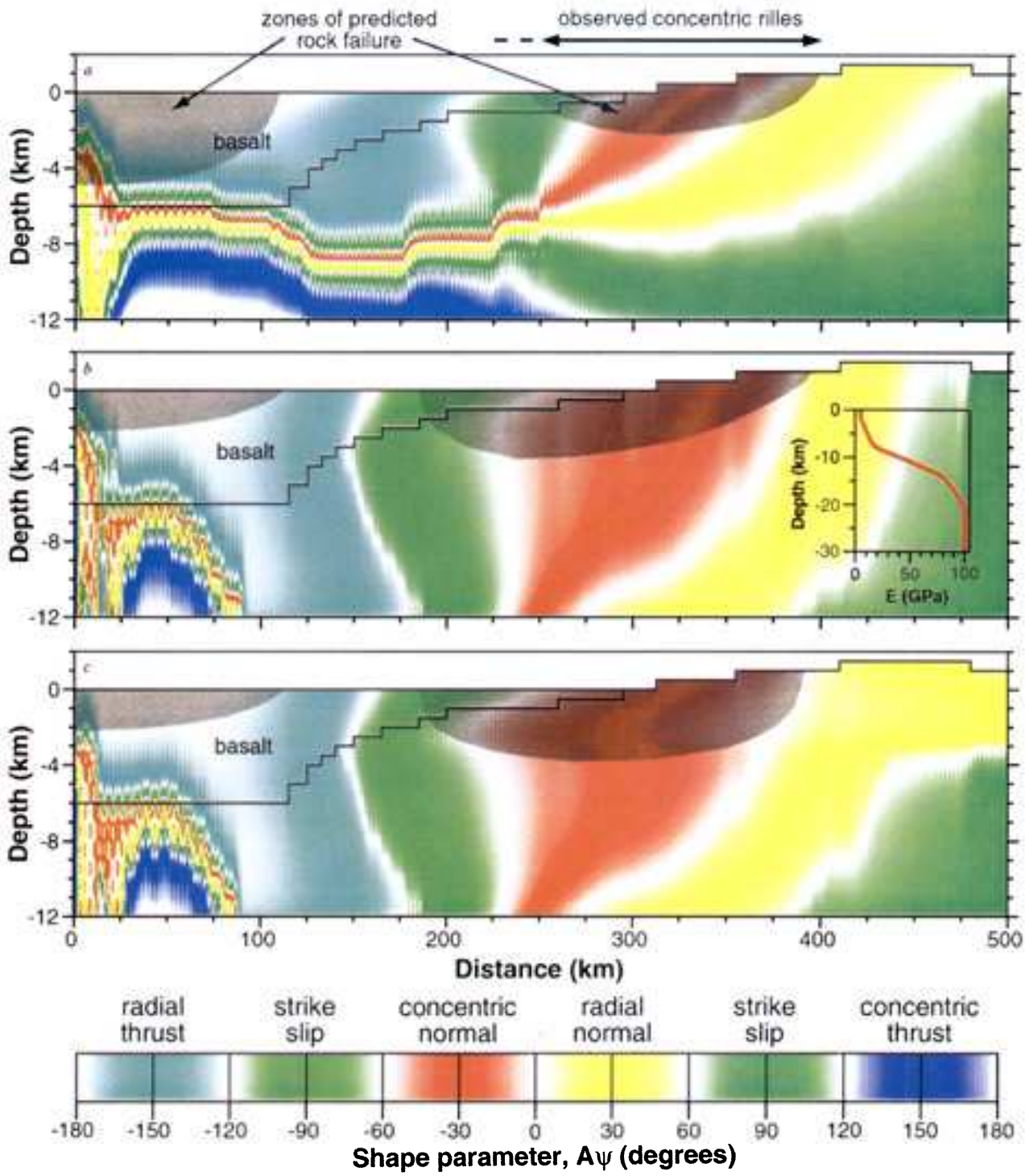

Plate 1. Styles of faulting predicted by the shape-parameter criterion and zones where flexural stresses exceed brittle strength ($P_f > 1$) for the Serenitatis basin at the time of rille formation due to flexure from a 6-km-deep mare load at the basin center and a lithospheric thickness of 25 km. (a) A model in which the lithosphere has a uniform Young's modulus of 10^{11} Pa, a cohesion c of 30 MPa, and an internal angle of friction ϕ of 25°. (b) A model with an elastically weak upper crust (inset) [*Pritchard and Stevenson*, 2000], c = 1 MPa, and ϕ_=25°. (c) A model with an elastically weak upper crust and a premare Poisson state of stress in the regolith (upper 3 km), c = 3 MPa, and ϕ_=25°. All models include lunar curvature.

concentric normal faults form, as observed, but not radial normal faults. The formation of thrust faults during later stages of mare emplacement is discussed below. For the model with a uniform lithospheric Young's modulus of 10^{11} Pa (Plate 1a), the observed faulting can be matched for a cohesive strength of 30 MPa and an internal angle of friction of 25^{o}. In the model with an elastically weak lithosphere (Plate 1b), observed faulting can be satisfied for a cohesion of 1 MPa and an internal angle of friction of 25^{o}. For the elastically weak model with an initial Poisson state of stress in the regolith (Plate 1c), a cohesion of 3 MPa and an internal angle of friction of 25^{o} satisfies observations. The initial Poisson-state model leads to a higher inferred cohesive strength because of prefill differential stresses.

Regardless of the modeled Young's modulus, the models in Plate 1 show that the predicted zone of strike-slip faulting invariably resides at the edge of the region in which flexural stresses are sufficient to induce rock failure. Thus the width of the annulus around mascon basins in which strike-slip faulting would be predicted to occur is usually a subset of the region in which strike-slip faulting is the preferred faulting style. For example, although a strike-slip faulting style is predicted for a 50-km-wide annulus around the Serenitatis basin for the high-elastic-modulus model shown in Figure 14a, only about half of this width experiences stress levels that are sufficient to induce failure. Thus we would only predict a 25-km-wide annulus of strike-slip faulting at the edge of Serenitatis at the time of rille formation. Note, however, that this region of predicted strike-slip faulting is subsequently covered by younger flows, as shown in Plate 2, a situation that also holds for the cases shown in Plates 1b and 1c. Thus no strike-slip faulting is predicted to be observable around Serenitatis at present.

To infer the strength characteristics of mare basalt, we consider models of mare ridge formation in response to loading by a younger unit of mare basalt emplaced after rille formation had ceased. As previously noted, the topmost layer of mare basalt experiences flexural stresses due only to the subsidence induced by its own load. Thus flexural stress levels in the youngest basalt load are lower than in the surrounding crust, which experiences subsidence due to the full mare load. This situation is compounded by the inferred weak elastic modulus of near-surface mare basalt at present [*Pritchard and Stevenson*, 2000], which serves to minimize stress levels. If a 2-km-thick unit of basalt of such modulus were emplaced on top of the 6-km-thick unit that already subsided, the resulting additional flexural stresses would not be sufficient to induce rock failure within the top unit unless it were both cohesionless and had a very low internal angle of friction (5^{o}- 10^{o}). However, if the younger mare basalt had a relatively high elastic modulus at the time of its emplacement and subsequent subsidence, then flexural stress levels would have been sufficiently high for rock failure to occur with a brittle failure envelope similar to that used for the nonmare crust.

Regions of predicted failure and styles of a faulting after flexure in response to the emplacement of an elastically strong 2-km-thick younger layer of mare basalt on top of an older 6-km-thick unit within the Serenitatis basin are shown in Plate 2a. With the higher assumed elastic modulus, faulting of the top mare basalt unit can be explained by a brittle strength envelope with c = 3 MPa and $\phi = 25^{o}$, values similar to those inferred for the surrounding non-mare crust. This model does not explain the radial extent of observed mare ridges, however, or the lack of rille formation. Modifications to the model to account for these observations are discussed next.

4.3. Inferred Lithosphere Thickness and Global Compression

Lithospheric thickness beneath the Serenitatis basin at the time of rille formation was determined by considering several models of varying thickness and noting which model best predicted the location of observed concentric rilles. A lithospheric thickness of 25 km (Plate 1) best explains observed rille locations. This thickness corresponds to the lower end of the 25-50 km range suggested by *Solomon and Head* [1979] and the 30-60 km range suggested by *Comer et al.* [1979]. The difference in results between our study and this previous work is due to the error mentioned above in the sign of the membrane stress used in the analytical solutions. Models with a lithospheric thickness greater than 25 km lead to predictions of strike-slip faulting in the region where concentric normal faulting is observed. For instance, a lithospheric thickness of 50 km leads to predicted strike-slip faulting in the distance range 225 to 325 km from basin center, whereas concentric rilles are observed in the range 250 to 400 km from basin center.

The observation that mare ridges overlie older rilles on the flank of Serenitatis suggests that the lunar lithosphere thickened between these two epochs, or a global horizontal compressive stress field was superimposed on the region after rille formation, or both [*Solomon and Head*, 1979]. To determine the lithospheric thickness at the time of youngest ridge formation, we return to models in which a 2-km-thick unit of younger mare basalt is emplaced on top of an older 6-km-thick unit after subsidence due to the older unit had achieved steady state. We consider models in which the lithosphere thickness increased from 25 km at the time of rille formation to 50, 75, and 100 km thick at the time of youngest ridge formation.

Two constraints guide the choice of lithosphere thickness at the time of youngest ridge formation. The first is that the total subsidence induced by the emplacement of the youngest (top) layer of mare basalt in the Serenitatis basin does not appear to exceed ~400 m on the basis of either Apollo-era topographic data [*Solomon and Head*, 1979] or Clementine altimetry (G. A. Neumann, personal communication, 2000). Central subsidence following emplacement of the younger basalt unit is calculated to be 700, 350, and 250 m for models with 50-, 75-, and 100-km-thick lithosphere, respectively. Given that the observed 400 m of relief is an upper bound on subsidence, the lithosphere thickness was probably at least ~70 km at the time of youngest ridge formation. That this thickness is considerably greater than the 25-km value inferred for the earlier time of rille formation is presumably the result of cooling and thickening of the lithosphere beneath the basin region [*Solomon and Head*, 1979, 1980].

The second constraint on lithospheric thickness is that mare ridges are observed to form as far as 300 km from the center of the Serenitatis basin [*Solomon and Head*, 1979]. In our models, thrust faulting is calculated to be the preferred style of faulting out to 175, 225, and 300 km from the basin center for 50-, 75-, and 100-km-thick lithospheres, respectively. However, differential stresses are insufficient to

induce faulting to these ranges. For the 75-km-thick lithosphere case (Plate 2a), differential stress levels are sufficient to induce thrust faulting only to ~180 km from the basin center. For the 100-km-thick lithosphere, differential stresses are sufficient to induce thrust faulting only to 150 km from the basin center. Thus none of the considered models can explain thrust faulting to 300 km distance from the basin center, as is observed.

In addition, all of these models predict a region of normal faulting at the edge of Serenitatis at the time of ridge formation. However, rille formation is inferred to have ceased by the time of emplacement of the youngest mare units. The lack of observed normal faulting at the time of youngest ridge formation could potentially be explained by lower stress levels after earlier normal faulting. Predicted stress resulting from the emplacement of only the youngest mare unit are not sufficient to induce failure in the normal faulting region (Plate 2b). For such a model to be appropriate, however, most flexural stresses induced by emplacement of the older basalt units must have been relieved by the faulting [*Neumann and Zuber*, 1995]. The model shown in Plate 2a is based on the assumption that none of the earlier flexural stresses were relieved by faulting. An intermediate solution is presumably most likely.

The inability of subsidence models to predict thrust faulting to 300-km distance from the Serenitatis basin center leads us to conclude that faulting around Serenitatis must have been influenced by an additional contribution to the stress field. One possibility is the superposition of compressional stresses due to global contraction of the lunar surface accompanying cooling of the lunar interior [*Solomon and Chaiken*, 1976; *Solomon*, 1977]. The accumulation of global horizontal compressive stress is inferred to have begun prior to the cessation of rille formation and to have continued through the time of the emplacement of the youngest mare basalt [*Solomon and Head*, 1979]. The peak compressive global stress following cessation of heavy bombardment was estimated by *Solomon and Head* [1979] to be at most 100 MPa, a value just small enough to be consistent with the absence of Moon-wide lithospheric failure (for a lithospheric Young's modulus of 10^{11} Pa).

We superimposed this horizontal compressive stress (in proportion to the local Young's modulus) to the Serenitatis model of Plate 2a. Such superposition is appropriate if the most distal mare ridges in the Serenitatis region formed well after volcanism had ceased. The predicted styles of faulting and regions of failure for this model are shown in Plate 2c. Note that the style of thrust faulting predicted throughout much of youngest mare load has no preferred orientation. Thus the observed mixture of concentric and radially oriented mare ridges may be a consequence of both the load history and a superimposed global compressional stress. Plate 2c shows surface thrust faulting to be predicted throughout the mare, with the exception of the exposed older basalt units 270 to 300 km from the basin center. Stresses in this region, predicted to lead to strike-slip faulting, are strongly influenced by flexure in response to the older mare units. Modest relief of the stress levels by earlier normal faulting, however, would be sufficient to change the predicted mode of failure to thrust faulting for this distal region. Our conclusion that the youngest mare ridges in Serenitatis formed at a time when the elastic lithosphere was at least 70 km thick and when there was a superposed state of global compression is consistent with the analytical results of *Solomon and Head* [1979, 1980].

5. Conclusions

The style of faulting of a planetary lithosphere in response to an axisymmetric surface load can be understood by comparing calculated flexural stresses from numerical models to a faulting-style criterion. Previous analytical and elastic plate models, together with the *Anderson* [1951] faulting criterion, did a remarkably good job of explaining the observed locations of rilles and mare ridges around lunar mascon basins as a function of lithospheric thickness. Such models also predict an annulus of strike-slip faulting, however, which is not observed. In addition to this strike-slip faulting paradox, previous models predict radially oriented thrust faults away from the basin center, whereas a mixture of radially and concentrically oriented ridges is observed. Our models demonstrate that the strike-slip faulting paradox and the prediction of predominantly radially oriented ridges result from oversimplifications in both the previous numerical models and the Anderson faulting criterion.

Viscoelastic finite element models of lunar mascon basins that include the effect of lunar curvature, heterogeneous crustal strength and initial stress conditions, and multistaged load histories yield at most small widths to the predicted annulus of strike-slip faulting. The width of a strike-slip zone shrinks further with recognition that strike-slip faulting, i.e., sets of conjugate shear fractures trending along Archimedean spirals, will be difficult to observe if significant dip-slip components to faulting are also present. Use of a faulting-style criterion such as the shape parameter of *Simpson* [1997], which takes into account regions of transitional faulting, predicts a zone of purely strike-slip faulting about half as wide as that predicted by the Anderson criterion. Furthermore, strike-slip faulting should be observable only in regions in which flexural stresses are sufficient to induce rock failure. Because strike-slip faulting around mascon loads represents a transition between compressional and extensional provinces where differential stresses tend to be low, differential stresses in much of the predicted strike-slip region do not lead to failure.

The observed mix of concentric and radial thrust faulting in some mare regions, at odds with previous models that predict only radial orientations away from the basin center, may be partly explained by multi-stage emplacement of mare basalt units. Multiple episodes of mare volcanism lead to the prediction that neither concentric nor radial orientations of thrust faults are preferred even hundreds of kilometers from the basin center.

Detailed models of the Serenitatis basin suggest that the elastic lithosphere beneath the basin was 25 km thick at the time rille formation and 75 km thick at the time of youngest mare ridge formation. The radial extent of observed mare ridges and the inferred cessation of rille formation prior to the end of mare basalt emplacement are consistent with the hypothesis that uniform horizontal compression associated with global cooling and contraction of the lunar interior was superimposed on the local stress field produced by mascon loading.

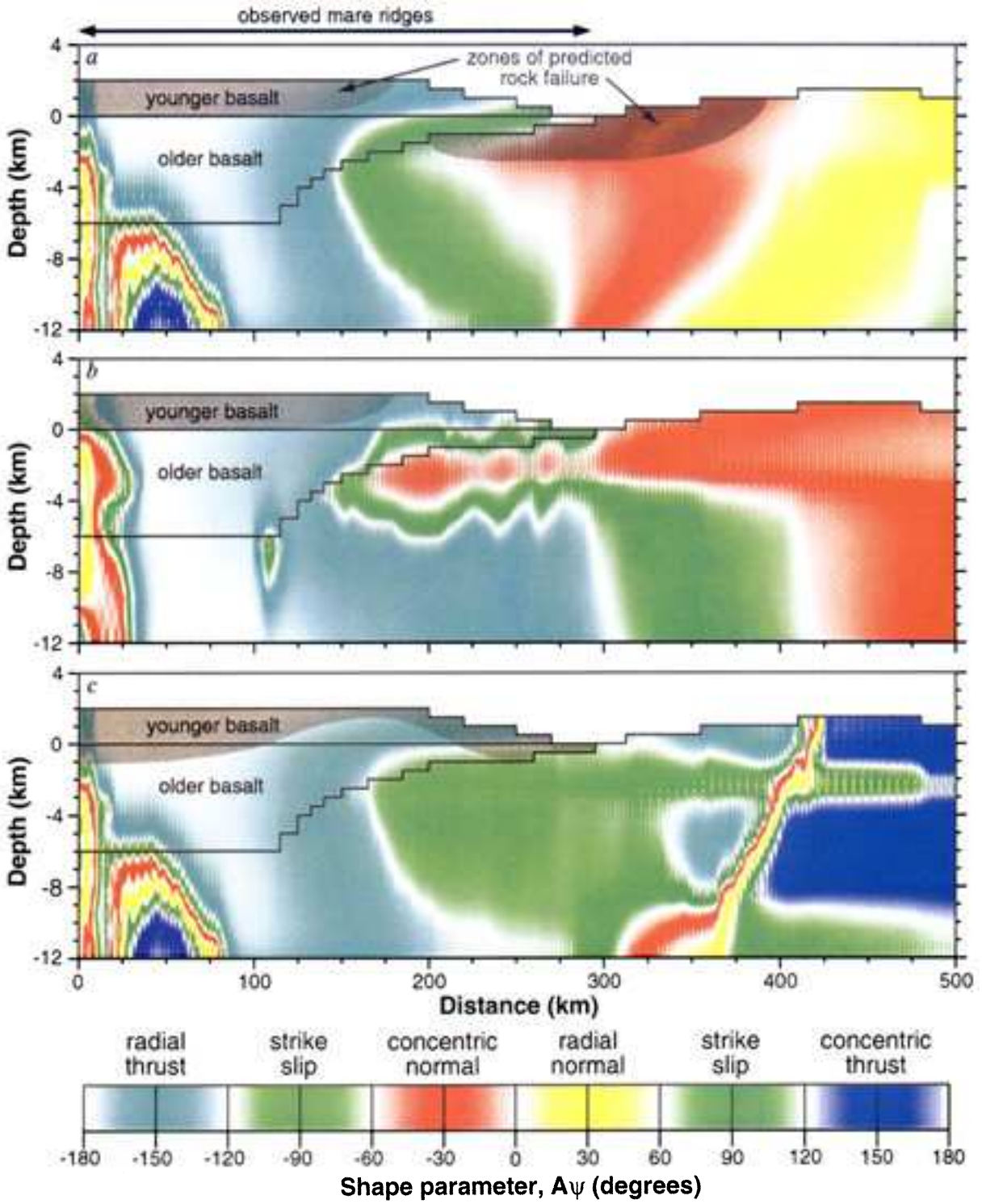

Plate 2. Styles of faulting predicted by the shape-parameter criterion and zones where flexural stresses exceed brittle strength ($P_f > 1$) for the Serenitatis basin at the time of younger mare ridge formation. In these models, flexural stresses are based on a 6-km-deep central mare load (older basalt units) emplaced on a 25-km-thick lithosphere, followed by an additional 2-km-deep central mare load (younger basalt units) emplaced on a 75-km-thick lithosphere. (a) Result of the combined emplacement of both sets of mare basalt units. (b) Result of the emplacement of only the younger mare basalt units. (c) Result of the combined emplacement of both sets of mare basalt units and a superimposed global horizontal compressive stress (see text). All models include an elastically strong younger basalt load, an elastically weak upper crust and older basalt load, and a premare Poisson state of stress in the regolith (upper 3 km), c = 3 MPa, and ϕ_=25^{o}. All models include lunar curvature.

Acknowledgments. We thank Patrick McGovern and Matt Golombek for helpful discussions, Sandy Keiser for computer support, Greg Neumann for Clementine data, and Maria Zuber for a constructive review of an earlier draft. This research was supported by NASA grant NAG 5–4077.

References

Anderson, E. M., *The Dynamics of Faulting*, 206 pp., Oliver and Boyd, Edinburgh, 1951.

Bowin, C., B. Simon, and W. R. Wollenhaupt, Mascons: A two-body solution, *J. Geophys. Res., 80*, 4947-4955, 1975.

Bratt, S. R., S. C. Solomon, J. W. Head, and C. H. Thurber, The deep structure of lunar basins: Implications for basin formation and modification, *J. Geophys. Res., 90*, 3049-3064, 1985a.

Bratt, S. R., S. C. Solomon, and J. W. Head, The evolution of impact basins; cooling, subsidence, and thermal stress, *J. Geophys. Res., 90*, 12,415-12,433, 1985b.

Brotchie, J. F., Flexure of a liquid-filled spherical shell in a radial gravity field, *Mod. Geol., 3*, 15-23, 1971.

Budney, C. J., and P. G. Lucey, Basalt thickness in Mare Humorum: The crater excavation method, *J. Geophys. Res., 103*, 16,855-16,870, 1998.

Byerlee, J. D., Frictional characteristics of granite under high confining pressure, *J. Geophys. Res., 72*, 3639-3648, 1967.

Celerier, B., Tectonic regime and slip orientation of reactivated faults, *Geophys. J. Int., 121*, 143-161, 1995.

Comer, R. P., S. C. Solomon, and J. W. Head, Elastic lithospheric thickness on the Moon from mare tectonic features: A formal inversion, *Proc. Lunar Planet. Sci. Conf. 10th*, 2441-2463, 1979.

Comer, R. P., S. C. Solomon, and J. W. Head, Mars: Thickness of the lithosphere from the tectonic response to volcanic loads, *Rev. Geophys., 23*, 61-92, 1985.

Conel, J. E., and G. B. Holstrom, Lunar mascons: A near-surface interpretation, *Science, 162*, 1403-1405, 1968.

Goins, N. R., A. M. Dainty, and M. N. Toksöz, Lunar seismology: The internal structure of the Moon, *J. Geophys. Res., 86*, 5061-5074, 1981.

Golombek, M. P., Fault type predictions from stress distributions on planetary surfaces: Importance of fault initiation depth, *J. Geophys. Res., 90*, 3065-3074, 1985.

Golombek, M. P., and G. E. McGill, Grabens, basin tectonics, and the maximum total expansion of the Moon, *J. Geophys. Res., 88*, 3563-3587, 1983.

Guiraud, M., O. Laborde, and H. Philip, Characterization of various types of deformation and their corresponding deviatoric stress tensors using microfault analysis, *Tectonophysics, 170*, 289-316, 1989.

Hall, J. L., S. C. Solomon, and J. W. Head, Elysium region, Mars: Tests of lithospheric loading models for the formation of tectonic features, *J. Geophys. Res., 91*, 11,377-11,392, 1986.

Head, J. W., Morphology and structure of the Taurus-Littrow highlands (Apollo 17): Evidence for their origin and evolution, *Moon, 9*, 355-395, 1974a.

Head, J. W., Lunar dark-mantle deposits: Possible clues to the distribution of early mare deposits, *Proc. Lunar Sci. Conf. 5th*, 207-222, 1974b.

Head, J. W., Serenitatis multi-ringed basin: Regional geology and basin ring interpretation, *Moon Planets, 21*, 439-462, 1979.

Head, J. W., J. B. Adams, T. B. McCord, C. Pieters, and S. Zisk, Regional stratigraphy and geological history of Mare Crisium, in *Mare Crisium: The View From Luna 24*, edited by R. B. Merrill and J. J. Papike, pp. 43-74, Pergamon, Tarrytown, New York, 1978.

Hoek, E., and E. T. Brown, Empirical strength criterion for rock masses, *J. Geotech. Eng. Div. Am. Soc. Civ. Eng., 106*, 1013-1035, 1980.

Howard, K. A., and W. R. Muehlberger, Lunar thrust faults in the Taurus-Littrow region, in *Apollo 17 Preliminary Science Report, NASA Spec. Publ., SP-330*, 31-22—31-25, 1973.

Howard, K. A., M. H. Carr, and W. R. Muehlberger, Basalt stratigraphy of southern Mare Serenitatis, in *Apollo 17 Preliminary Science Report, NASA Spec. Publ., SP-330*, 29-1—29-12, 1973.

Janes, D. M., and H. J. Melosh, Tectonics of planetary loading: A general model and results, *J. Geophys. Res., 95*, 21,345-21,355, 1990.

Janes, D. M., S. W. Squyres, D. L. Bindschadler, G. Baer, G. Schubert, V. L. Sharpton, and E. R. Stofan, Geophysical models for the formation and evolution of coronae on Venus, *J. Geophys. Res., 97*, 16,055-16,067, 1992.

Landau, L. D., and E. M. Lifshitz, *Theory of Elasticity*, 289 pp., Pergamon, Tarrytown, New York, 1970.

Lucchitta, B. K., Topography, structure, and mare ridges in southern Mare Imbrium and northern Oceanus Procellarum, *Proc. Lunar Sci. Conf. 8th*, 2691-2703, 1977.

Lucchitta, B. K., and J. A. Watkins, Age of graben systems on the Moon, *Proc. Lunar Planet. Sci. Conf. 9th*, 3459-3472, 1978.

Maxwell, T. A., F. El-Baz, and S. H. Ward, Distribution, morphology, and origin of ridges and arches in Mare Serenitatis, *Geol. Soc. Am. Bull., 86*, 1273-1278, 1975.

McGovern, P. J., and S. C. Solomon, State of stress, faulting, and eruption characteristics of large volcanoes on Mars, *J. Geophys. Res., 98*, 23,553-23,579, 1993.

McGovern, P. J., and S. C. Solomon, Growth of large volcanoes on Venus: Mechanical models and implications for structural evolution, *J. Geophys. Res., 103*, 11,071-11,101, 1998.

Melosh, H. J., On the origin of fractures radial to lunar basins, *Proc. Lunar Sci. Conf. 7th*, 2967-2982, 1976.

Melosh, H. J., The tectonics of mascon loading, *Proc. Lunar Planet. Sci. Conf. 9th*, 3513-3525, 1978.

Melosh, H. J., *Impact Cratering, A Geological Process*, 245 pp., Oxford Univ. Press, New York, 1989.

Melosh, H. J., and A. Raefsky, The dynamic origin of subduction zone topography, *Geophys. J. R. Astron. Soc., 60*, 333-354, 1980.

Melosh, H. J., and C. A. Williams, Mechanics of graben formation in crustal rocks: A finite-element analysis, *J. Geophys. Res., 94*, 13,961-13,973, 1989.

Muehlberger, W. R., Structural history of southeastern Mare Serenitatis and adjacent highlands, *Proc. Lunar Sci. Conf. 5th*, 101-110, 1974.

Muller, P. M., and W. L. Sjogren, Mascons: Lunar mass concentrations, *Science, 161*, 680-684, 1968.

Nakamura, Y., G. V. Latham, H. J. Dorman, A.-B. K. Ibrahim, J. Koyama, and P. Horvath, Shallow moonquakes: Depth, distribution and implications as to the present state of the lunar interior, *Proc. Lunar Planet. Sci. Conf. 10th*, 2299-2309, 1979.

Neumann, G. A., and M. T. Zuber, A continuum approach to the development of normal faults, in *Rock Mechanics*, edited by J. Daemen and R. Schultz, pp. 191-198, Balkema, Rotterdam, 1995.

Neumann, G. A., M. T. Zuber, D. E. Smith, and F. G. Lemoine, The lunar crust: Global structure and signature of major basins, *J. Geophys. Res., 101*, 16,841-16,863, 1996.

Philip, H., Plio-Quaternary evolution of the stress field in Mediterranean zones of subduction and collision, *Ann. Geophys., Ser. B, 5*, 301-319, 1987.

Phillips, R. J., and J. Dvorak, The origin of lunar mascons: Analysis of the Bouguer gravity associated with Grimaldi, in *Proceedings of the Conference on Multi-ring Basins: Formation and Evolution*, edited by P. H. Schultz and R. B. Merrill, pp. 91–104, Pergamon, Tarrytown, New York, 1981.

Phillips, R. J., and T. A. Maxwell, Lunar Sounder revisited: Stratigraphic correlations and structural inferences (abstract), *Lunar Planet. Sci., 9*, 890-892, 1978.

Phillips, R. J., J. E. Conel, E. A. Abbot, W. L. Sjogren, and J. B. Morton, Mascons: Progress toward a unique solution for mass distribution, *J. Geophys. Res., 77*, 7106-7114, 1972.

Pieters, C., J. W. Head, T. B. McCord, J. B. Adams, and S. Zisk, Geochemical and geological units of Mare Humorum: Definition using remote sensing and lunar sample information, *Proc. Lunar Sci. Conf. 6th*, 2689-2710, 1975.

Pieters, C., J. W. Head, J. B. Adams, T. B. McCord, S. Zisk, and J. L. Whitford-Stark, Late high-titanium basalts of the western maria: Geology of the Flamsteed region of Oceanus Procellarum, *J. Geophys. Res., 85*, 3913-3938, 1980.

Pritchard, M. E., and D. J. Stevenson, Thermal aspects of a lunar origin by giant impact, in *Origin of the Earth and Moon*, edited by R. M. Canup and K. Righter, pp. 179-196, Univ. of Ariz. Press, Tucson, 2000.

Pullan, S., and K. Lambeck, Mascons and loading of the lunar lithosphere, *Proc. Lunar Planet. Sci. Conf. 12th*, 853-865, 1981.

Scholz, C. H., *The Mechanics of Earthquakes and Faulting*, 439 pp., Cambridge Univ. Press, New York, 1990.

Schultz, R. A., and M. T. Zuber, Observations, models, and mechanisms of failure of surface rocks surrounding planetary surface loads, *J. Geophys. Res., 99*, 14,691-14,702, 1994.

Secor, D. T., Jr., Role of fluid pressure in jointing, *Am. J. Sci., 263*, 633-646, 1965.

Simpson, R. W., Quantifying Anderson's fault types, *J. Geophys. Res., 102*, 17,909-17,919, 1997.

Solomon, S. C., The relationship between crustal tectonics and internal evolution in the Moon and Mercury, *Phys. Earth Planet. Int., 15*, 135-145, 1977.

Solomon, S. C., and J. Chaiken, Thermal expansion and thermal stress in the Moon and terrestrial planets: Clues to early thermal history, *Proc. Lunar Sci Conf. 7th*, 3229-3243, 1976.

Solomon, S. C., and J. W. Head, Vertical movement in mare basins: Relation to mare emplacement, basin tectonics, and lunar thermal history, *J. Geophys. Res., 84*, 1667-1682, 1979.

Solomon, S. C., and J. W. Head, Lunar mascon basins: Lava filling, tectonics, and evolution of the lithosphere, *Rev. Geophys., 18*, 107-141, 1980.

Squyres, S. W., D. M. Janes, G. Baer, D. L. Bindschadler, G. Schubert, V. L. Sharpton, and E. R. Stofan, The morphology and evolution of coronae on Venus, *J. Geophys. Res., 97*, 13,611-13,634, 1992.

Stofan, E. R., V. L. Sharpton, G. Schubert, G. Baer, D. L. Bindschadler, D. M. Janes, and S. W. Squyres, Global distribution and characteristics of coronae and related features on Venus: Implications for origin and relation to mantle processes, *J. Geophys. Res., 97*, 13,347-13,378, 1992.

Turcotte, D. L., and G. Schubert, *Geodynamics: Applications of Continuum Physics to Geological Problems*, 450 pp., John Wiley, New York, 1982.

Turtle, E. P., and H. J. Melosh, Stress and flexural modeling of the Martian lithospheric response to Alba Patera, *Icarus, 126*, 197-211, 1997.

Whitford-Stark, J. L., and J. W. Head, Stratigraphy of Oceanus Procellarum basalts: Sources and styles of emplacement, *J. Geophys. Res., 85*, 6579-6609, 1980.

Wilhelms, D. E., The geological history of the Moon, *U.S. Geol. Surv. Prof. Pap. 1348*, 302 pp., 1987.

Willemann, R. J., and D. L. Turcotte, The role of lithospheric stress in the support of Tharsis rise, *J. Geophys. Res., 87*, 9793-9801, 1982.

Williams, K. K., and M. T. Zuber, Measurement and analysis of lunar basin depths from Clementine altimetry, *Icarus, 131*, 107-122, 1998.

Willis, J. J., and V. L. Hansen, Conjugate shear fractures at "Ki Corona," southeast Parga Chasma, Venus (abstract), *Lunar Planet. Sci., 27*, 1443-1444, 1996.

Wise, D. U., and M. Y. Yates, Mascons as surface relief on a lunar "Moho," *J. Geophys. Res., 75*, 261-268, 1970.

Zuber, M. T., D. E. Smith, F. G. Lemoine, and G. A. Neumann, The shape and internal structure of the Moon from the Clementine mission, *Science, 266*, 1839-1843, 1994.

A. M. Freed and S. C. Solomon, Department of Terrestrial Magnetism, Carnegie Institution of Washington, 5241 Broad Branch Road, N. W., Washington, DC 20015 (freed@dtm.ciw.edu).

H. J. Melosh, Lunar and Planetary Laboratory, University of Arizona, Tucson, AZ 85721.

(Received August 7, 2000; revised April 6, 2001;
accepted April 25, 2001)